Basic research

Nephrology

Editor's choice

Metabolic profiles of IgA nephropathy, membranous nephropathy, and diabetic nephropathy

Yasin Abdi Saed[1], Lili Guo[2], Rongshan Li[2,3]*

[1]Department of Medicine, International College of Medicine and Pharmacy, Changsha Medical University, Changsha, China
[2]Key Laboratory of Kidney Disease, Precision Medicine Center, Shanxi Provincial People's Hospital, Shanxi Medical University, Taiyuan, China
[3]Department of Nephrology, Fifth Hospital of Shanxi Medical University (Shanxi Provincial People's Hospital), Taiyuan, China

Submitted: 12 February 2025; **Accepted:** 12 September 2025
Online publication: 8 February 2026

Arch Med Sci 2026; 22 (4): 2334–2352
DOI: https://doi.org/10.5114/aoms/210616
Copyright © 2026 Termedia & Banach

***Corresponding author:**
Rongshan Li
Department of Nephrology
Fifth Hospital of
Shanxi Medical University
(Shanxi Provincial
People's Hospital)
Key Laboratory of
Kidney Disease
Precision Medicine Center
Shanxi Provincial
People's Hospital
Shanxi Medical University
Taiyuan, China
E-mail: rongshanli@126.com

Abstract

Introduction: Immunoglobulin A nephropathy (IgAN), membranous nephropathy (MN), and diabetic nephropathy (DN) are prominent contributors to chronic kidney disease burden. Our main objective was to contribute to the understanding of the metabolic profiles of these three major types of nephropathies and identify potential metabolic biomarkers.
Material and methods: Kidney samples of 20 sex- and age-matched patients with biopsy-proven IgAN, MN, DN, and controls without any kidney diseases were included. Ultra-high-performance liquid chromatography–mass spectrometry analysis was conducted. The *t*-test was used to evaluate the statistical significance of the identified metabolites. Metabolic pathways were analyzed using the Kyoto Encyclopedia of Genes and Genomes (KEGG). Specificity, sensitivity, and area under the curve (AUC) were calculated to evaluate the predictive performance of metabolites.
Results: Among 557 identified differential metabolites, only 118 were found in all three comparison groups. Differential metabolites of IgAN vs. controls were significantly enriched in arachidonic acid metabolism, starch and sucrose metabolism, ferroptosis, and other pathways. In the DN group, metabolites were mainly enriched in phenylalanine, tyrosine and tryptophan biosynthesis, histidine metabolism, etc. MN-enriched pathways included steroid hormone biosynthesis, neuroactive ligand-receptor interaction, and bile secretion. In the positive mode, cumulative AUC values for comparison pairs IgAN vs. controls, MN vs controls, and DN vs controls were 0.965, 0.972, and 0.573, respectively, whereas in the negative mode the AUC values of all three pairs were slightly above 0.65.
Conclusions: IgAN, MN, and DN have similar but distinct metabolic profiles. Only positive node metabolites of IgAN and MN exhibited high predictive performance.
Key words: IgA nephropathy, membranous nephropathy, diabetic nephropathy, metabolomics, bioinformatics.

Introduction

Chronic kidney diseases (CKDs) include various conditions characterized by progressive loss of renal function, leading to significant morbidity and mortality worldwide [1, 2]. Among these, immunoglobulin A nephropathy (IgAN), membranous nephropathy (MN), and diabetic nephropathy (DN) are prominent contributors to CKD burden, each with distinct

Creative Commons licenses: This is an Open Access article distributed under the terms of the Creative Commons Attribution-NonCommercial-ShareAlike 4.0 International (CC BY -NC -SA 4.0). License (http://creativecommons.org/licenses/by-nc-sa/4.0/).

etiologies and pathological mechanisms [2]. IgAN is the most common type of primary glomerulonephritis globally, characterized by the deposition of IgA immune complexes in the glomerular mesangium [3]. MN, another leading cause of nephrotic syndrome in adults, is characterized by immune-mediated thickening of the glomerular basement membrane [4]. DN, a complication of diabetes mellitus, represents the most common cause of end-stage renal disease worldwide, driven by metabolic and inflammatory pathways induced by chronic hyperglycemia [5].

Metabolomics, an omics approach focused on the systematic study of small molecule metabolites within biological systems, has become an extremely popular approach to study the pathophysiological processes of various disorders, including CKDs [6–8]. Liquid chromatography–mass spectrometry (LC-MS), a robust analytical technique, provides high-resolution detection and quantification of metabolites, thereby enabling comprehensive profiling of metabolic alterations associated with disease states [9, 10]. In this study, we employed LC-MS-based metabolomics to investigate and compare the metabolic profiles of kidney tissues from IgAN, MN, and DN patients with healthy controls. Our main objective was to contribute to the understanding of the metabolic profiles of these three major types of nephropathies and identify potential metabolic biomarkers for early diagnosis and prompt treatment.

Material and methods

Data collection

A prospective sex- and age-matched cohort study was performed at Shanxi Provincial People's Hospital from June 2019 to June 2020. The goal was to include 20 patients with biopsy-proven IgAN (group A), MN (group B), DN (group C), and controls without any kidney diseases (group D). Exclusion criteria: age < 18 years old, BMI < 18 or > 24 kg/m^2, secondary nephropathy, autoimmune diseases, hepatitis, cirrhosis, malignancies, recent steroid or immunosuppression treatment within 6 months, or use of metabolic medications (e.g., statins, fibrates, ezetimibe, febuxostat, benzbromarone, compound α-ketoacid tablets, fish oil) within 7 days. The study was approved by the institutional ethics committee, and written informed consent was obtained from each patient.

Metabolite extraction

First, 100 mg of tissue was ground with liquid nitrogen. The resulting homogenate was then resuspended with a chilled solution of 80% methanol and 0.1% formic acid, followed by thorough vortexing. The samples were placed on ice for 5 min and centrifuged at 15,000 rpm and 4°C for 5 min. A portion of the supernatant was diluted with LC-MS grade water to achieve a final methanol concentration of 53%. These samples were transferred to a new Eppendorf tube and centrifuged again at 15,000 rpm and 4°C for 10 min. Finally, the supernatant was injected into the LC-MS system for analysis.

For liquid samples, 100 µl of sample with 400 µl of chilled methanol were mixed and vortexed. For cell samples, samples were mixed with 80% chilled methanol (four times the sample volume), vortexed well, and sonicated for 6 min. Sonication was repeated, after which the same steps as for tissue samples were followed.

Liquid chromatography-mass spectrometry analysis

Ultra-high-performance LC-MS analysis was conducted using a Vanquish LC system (Thermo Fisher, Germany) connected to an Orbitrap Q Exactive HF-X mass spectrometer (Thermo Fisher, Germany) at Novogene Co., Ltd. (Beijing, China). Samples were injected into a Hypersil Gold column (100 × 2.1 mm, 1.9 µm) using a 17-minute linear gradient at 0.2 ml/min flow rate. For positive polarity mode, eluent A was 0.1% formic acid in water, and eluent B was methanol. For negative polarity mode, eluent A was 5 mM ammonium acetate at pH 9.0, and eluent B was methanol. The solvent gradient was programmed as follows: 2% B for 1.5 min, 2–100% B over 12.0 min, 100% B for 14.0 min, 100–2% B for 14.1 min, and 2% B until 17 min. The mass spectrometer was operated in positive/negative polarity mode with a spray voltage of 3.2 kV, capillary temperature of 320°C, a sheath gas flow rate of 40 arb, and auxiliary gas flow rate of 10 arb.

Data processing and metabolite identification

The raw data files from the LC-MS were processed using Compound Discoverer 3.1 (CD3.1, Thermo Fisher) for peak alignment, peak picking, and quantification of each metabolite. Key parameters were set to a retention time tolerance of 0.2 min, mass tolerance of 5 ppm, signal intensity tolerance of 30%, a signal-to-noise ratio of 3, and a minimum intensity of 100,000. Peak intensities were normalized to the total spectral intensity. The normalized data were used to predict molecular formulas based on additive ions, molecular ion peaks, and fragment ions. Peaks were matched against mzCloud, mzVault, and MassList databases to obtain accurate qualitative and relative quantitative results. Statistical analyses were conducted using R Python and CentOS. The metabolites with a coefficient

of variance (CV) > 30% in the quality control (QC) samples were removed.

Data analysis

Metabolites were annotated using the Kyoto Encyclopedia of Genes and Genomes (KEGG), Human Metabolome Database (HMDB), and LIPID Maps databases. Principal component analysis (PCA) and partial least squares discriminant analysis (PLS-DA) were performed using metaX. Univariate analysis (*t*-test) was used to calculate statistical significance. Metabolites with VIP > 1, *p*-value < 0.05, and fold change (FC) ≥ 1.2 or ≤ 0.833 were considered differential metabolites. Data for clustering heat maps were normalized using z-scores of differential metabolites' intensity areas and plotted with the Pheatmap package in R. Correlations between differential metabolites were analyzed using the cor() function in R with the Pearson method, and significance was calculated with cor.mtest(). Metabolic pathways were analyzed using KEGG (hypergeometric test, adjusted by Benjamini and Hochberg method), and pathway enrichment was considered significant with a ratio of x/n > y/N and *p*-value < 0.05. Specificity and sensitivity were calculated, a receiver operating characteristic (ROC) curve was plotted, and area under the curve (AUC) values were calculated to assess the predictive performance of metabolites.

Results

Quality control

Pearson correlation revealed a high correlation among QC samples (Supplementary Figures S1 A, D). The peaks extracted from all the experimental and QC samples were subjected to PCA analysis after univariate scaling. As shown in the PCA plot, closely clustered QC samples indicate good stability of the whole method and high data quality. Except for QC samples in the positive mode, samples in every group were mixed with each other (Supplementary Figures S1 B, C, E, F).

Screening of differential metabolites

A total of 795 and 457 metabolites were identified in the positive and negative modes, respectively. In both positive and negative modes, the first two principal components capture a significant proportion of the variance in the data (23.28–28.32% for PC1 and 6.78–12.88% for PC2). However, all groups are mixed, indicating that the variance captured by the principal components does not significantly differentiate the groups (Figure 1). In contrast, PLS-DA revealed significant separation between each nephropathy group and control group (A vs. D, B vs. D, and C vs. D) in both modes (Figures 2 A–C, G–I). This is because PLS-DA uses group information to maximize the variance between groups, leading to better discrimination. Moreover, the corresponding permutation test plots support the statistical significance of the PLS-DA model (Figures 2 D–F, J–L). Importantly, the model is not overfitted, as evidenced by the following indicators: the R2 value is larger than the Q2 value, and the intercept of the Q2 regression line with the Y-axis is less than 0.

According to KEGG enrichment analysis, metabolites were mainly enriched in amino acid and lipid metabolism and involved in the digestive system (Figures 3 A, B). HMDB revealed that most of the metabolites were lipids and lipid-like molecules, organic acids and derivatives, organoheterocyclic compounds, and benzoids (Figures 3 C, D). LIPID MAPS annotation showed that metabolites were linked with steroids, isoprenoids, flavonoids, fatty acids and conjugates, etc. (Figures 3 E, F).

Table I shows the number of differential metabolites after application of cutoff values (VIP > 1, FC > 1.2 and FC < 0.833, *p*-value < 0.05) for each comparison pair. Volcano plots are illustrated in Figure 4. A total of 341 and 216 significantly differential metabolites were identified in the positive and negative modes, respectively, among which 71 and 47 metabolites were present in all three comparison groups (Supplementary Table SI and SII). Hierarchical clustering analysis was performed for all the differential metabolites among four groups and within each comparison pair (Supplementary Figure S2).

Correlation and enrichment analyses

Correlation analysis of metabolites was conducted to understand the relationships between individual metabolites within the dataset. Pearson correlation coefficients were calculated for all pairwise comparisons of metabolites, and the results are illustrated in Figure 5. In the positive mode, most of the metabolites were highly positively correlated with each other except for 4-phenyl-3-buten-2-one, (12Z)-9,10,11-trihydroxyoctadec-12-enoic acid, and PC (18:2/20:5) in the IgAN vs control pairwise comparison. In the negative node, many metabolite pairs exhibited a mild-to-moderate correlation. KEGG pathway enrichment analysis was used to identify the main biological functions of metabolites. Metabolites were found to be enriched in various pathways (Supplementary Table SIII). Based on the KEGG enrichment results, bubble charts were plotted (Figure 6).

Predictive modelling

Logistic regression was performed to evaluate the predictive performance of differential meta-

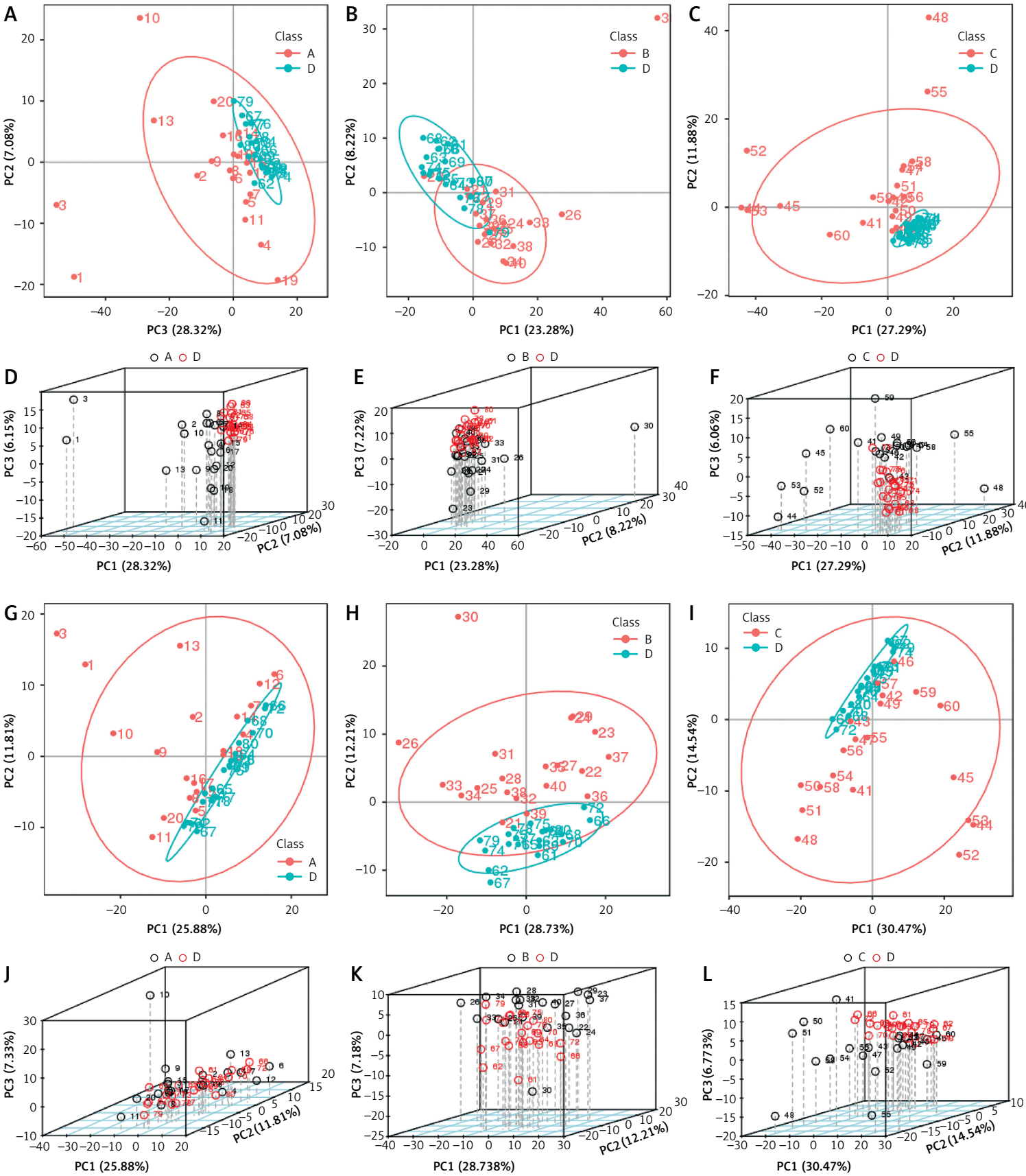


Figure 1. Principal component analysis (PCA) plots. **A** – IgA nephropathy (IgAN) vs. control pair (positive mode, 2 dimensions). **B** – Membranous nephropathy (MN) vs. control pair (positive mode, 2 dimensions). **C** – Diabetic nephropathy (DN) vs. control pair (positive mode, 2 dimensions). **D** – IgAN vs. control pair (positive mode, 3 dimensions). **E** – MN vs. control pair (positive mode, 3 dimensions). **F** – DN vs. control pair (positive mode, 3 dimensions). **G** – IgAN vs. control pair (negative mode, 2 dimensions). **H** – MN vs. control pair (negative mode, 2 dimensions). **I** – DN vs. control pair (negative mode, 2 dimensions). **J** – IgAN vs. control pair (negative mode, 3 dimensions). **K** – MN vs. control pair (negative mode, 3 dimensions). **L** – DN vs. control pair (negative mode, 3 dimensions)

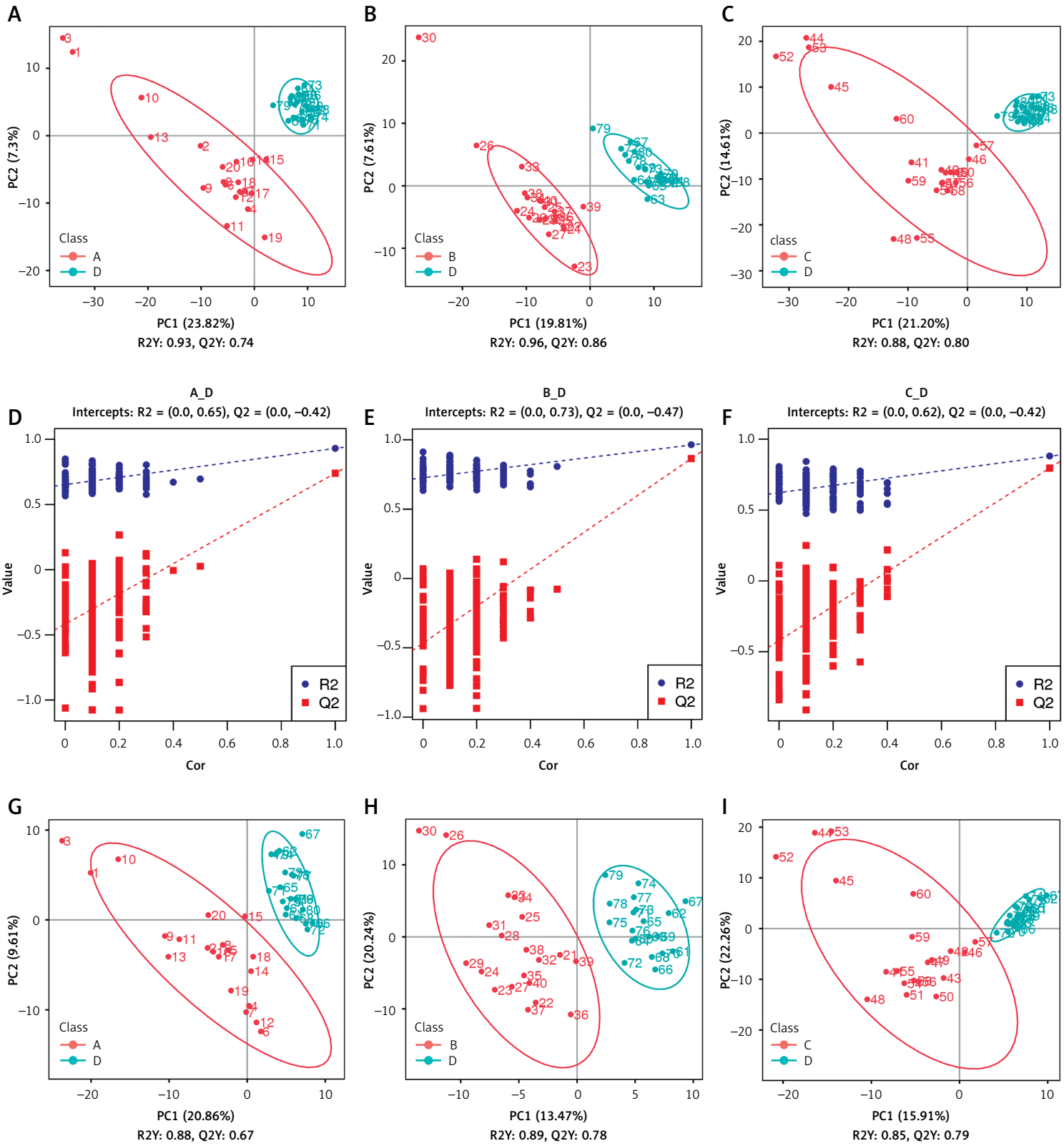


Figure 2. Partial least squares discriminant analysis. **A** – Principal component (PC) plot, IgA nephropathy (IgAN) vs. control pair (positive mode). **B** – PC plot, membranous nephropathy (MN) vs. control pair (positive mode). **C** – PC plot, diabetic nephropathy (DN) vs. control pair (positive mode). **D** – Permutation test (PT) plot, IgAN vs. control pair (positive mode). **E** – PT plot, MN vs. control pair (positive mode). **F** – PT plot, DN vs. control pair (positive mode). **G** – PC plot, IgAN vs. control pair (negative mode). **H** – PC plot, MN vs. control pair (negative mode). **I** – PC plot, DN vs. control pair (negative mode)

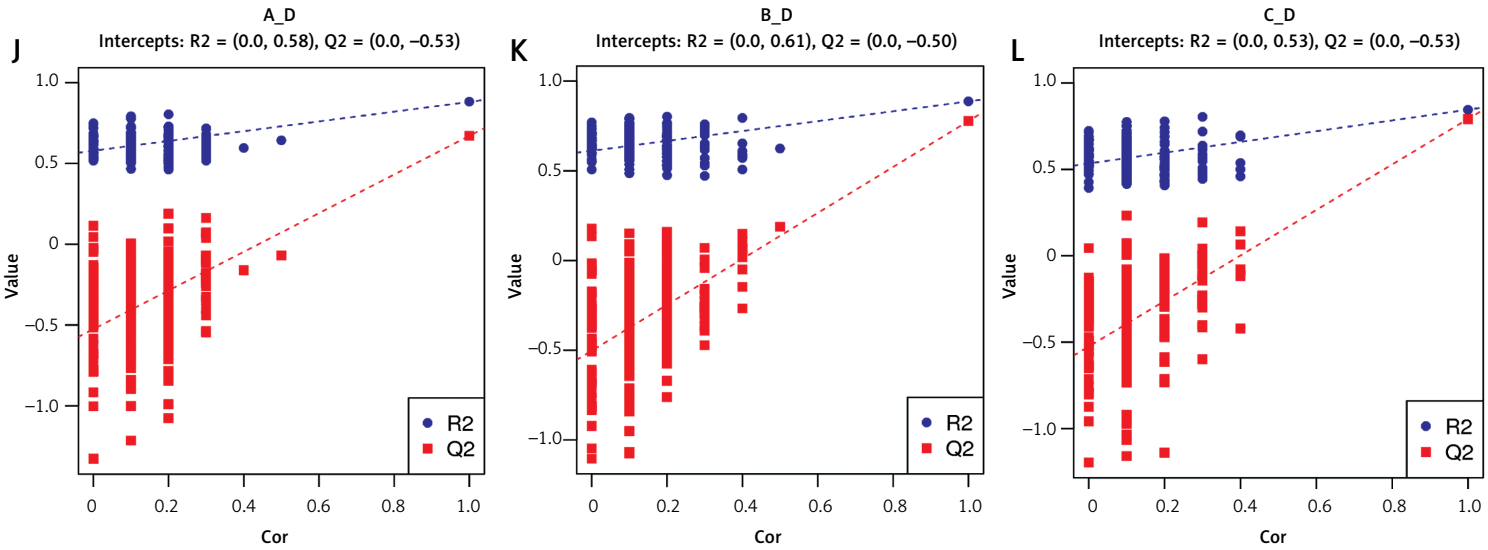


Figure 2. Cont. Partial least squares discriminant analysis. **J** – PT plot, IgAN vs. control pair (negative mode). **K** – PT plot, MN vs. control pair (negative mode). **L** – PT plot, DN vs. control pair (negative mode)

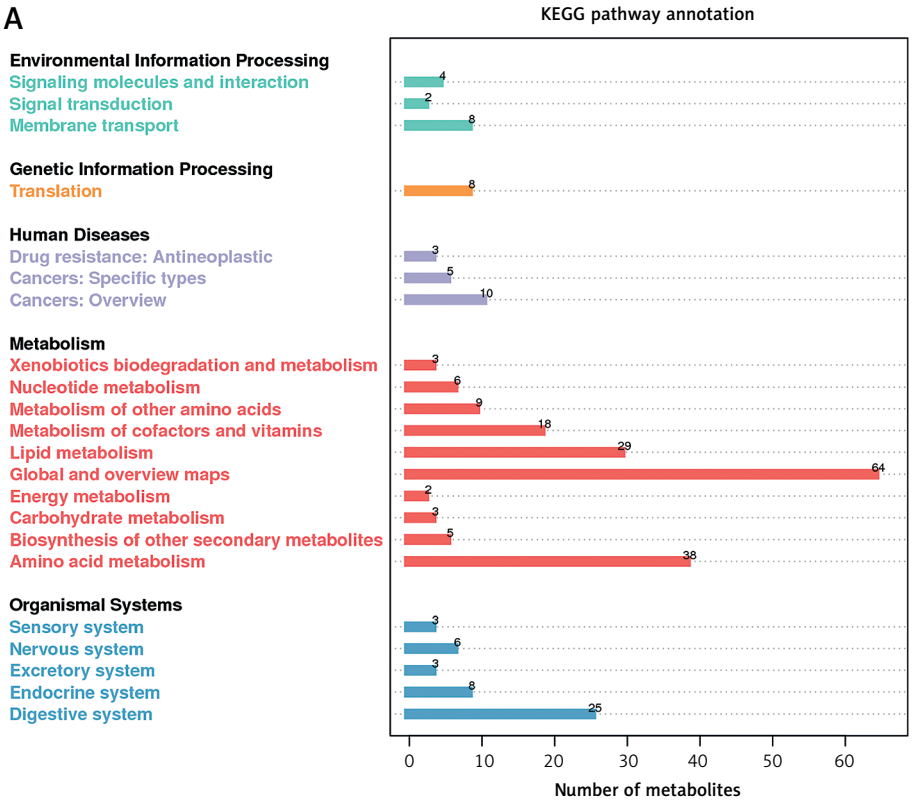
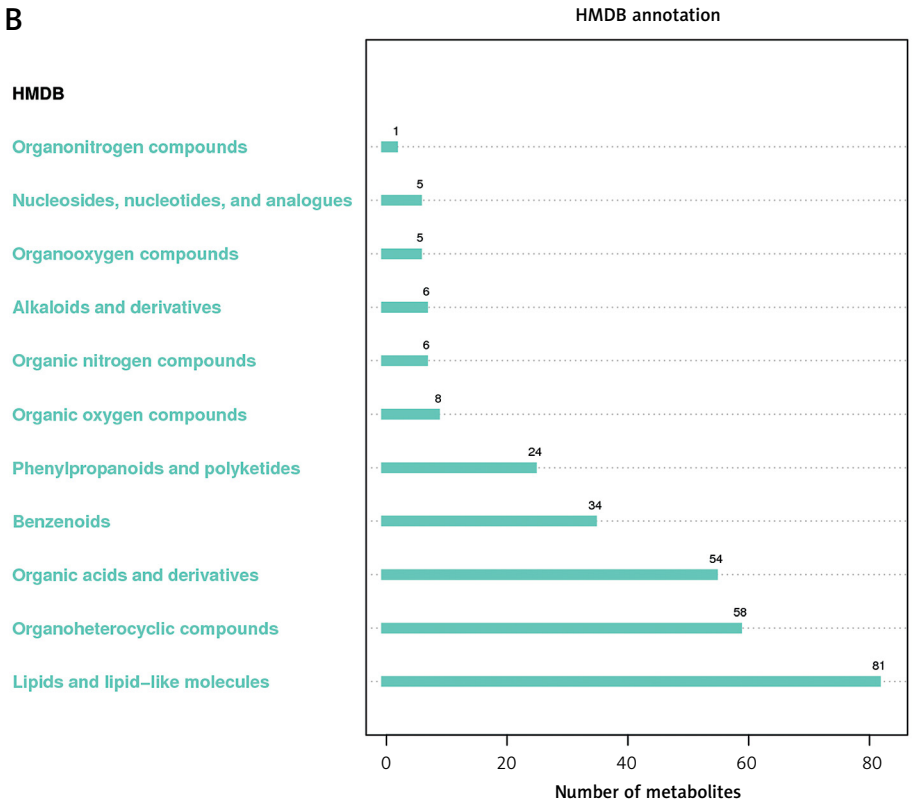


Figure 3. Metabolite annotation. **A** – Kyoto Encyclopedia of Genes and Genomes (KEGG) pathway annotation (positive mode)

bolites (Figure 7). In the positive mode, cumulative AUC values for comparison pairs IgAN vs controls and MN vs controls were 0.965 and 0.972, respectively. Thus, AUC values for the first two pairs indicate excellent discriminatory ability as shown by strong performance in distinguishing between IgAN or MN and controls. In contrast, the AUC value for DN was 0.573, occasionally falling below the random classifier curve. In the negative mode, the AUC values of the three comparison pairs



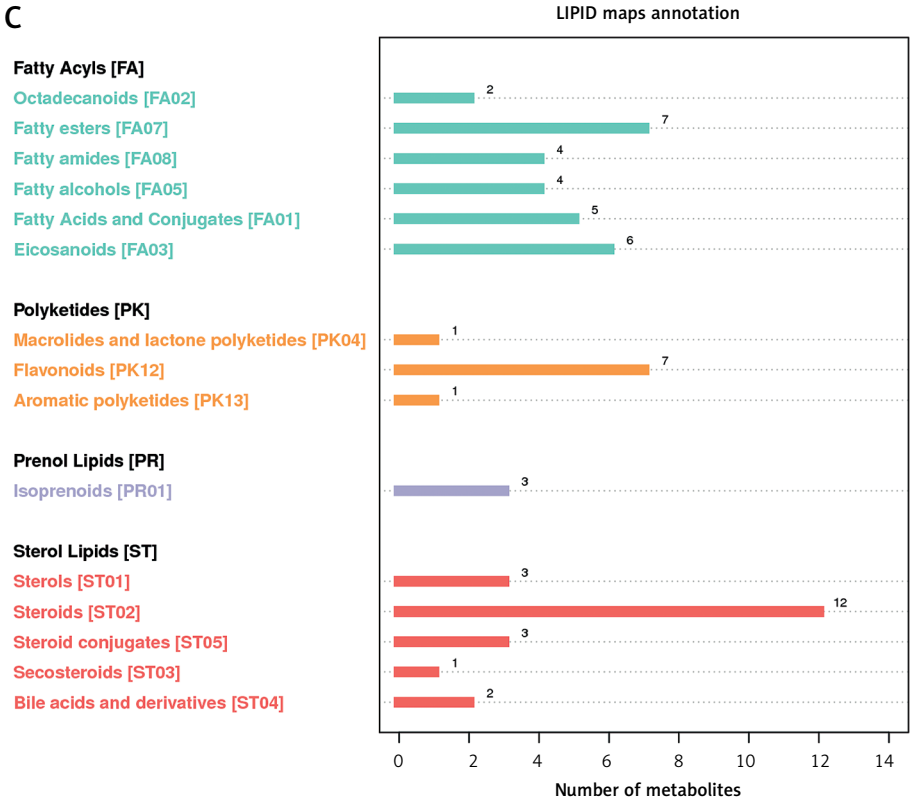


Figure 3. Cont. Metabolite annotation. **B** – Human Metabolome Database (HMDB) annotation (positive mode). **C** – LIPID Maps annotation (positive mode)

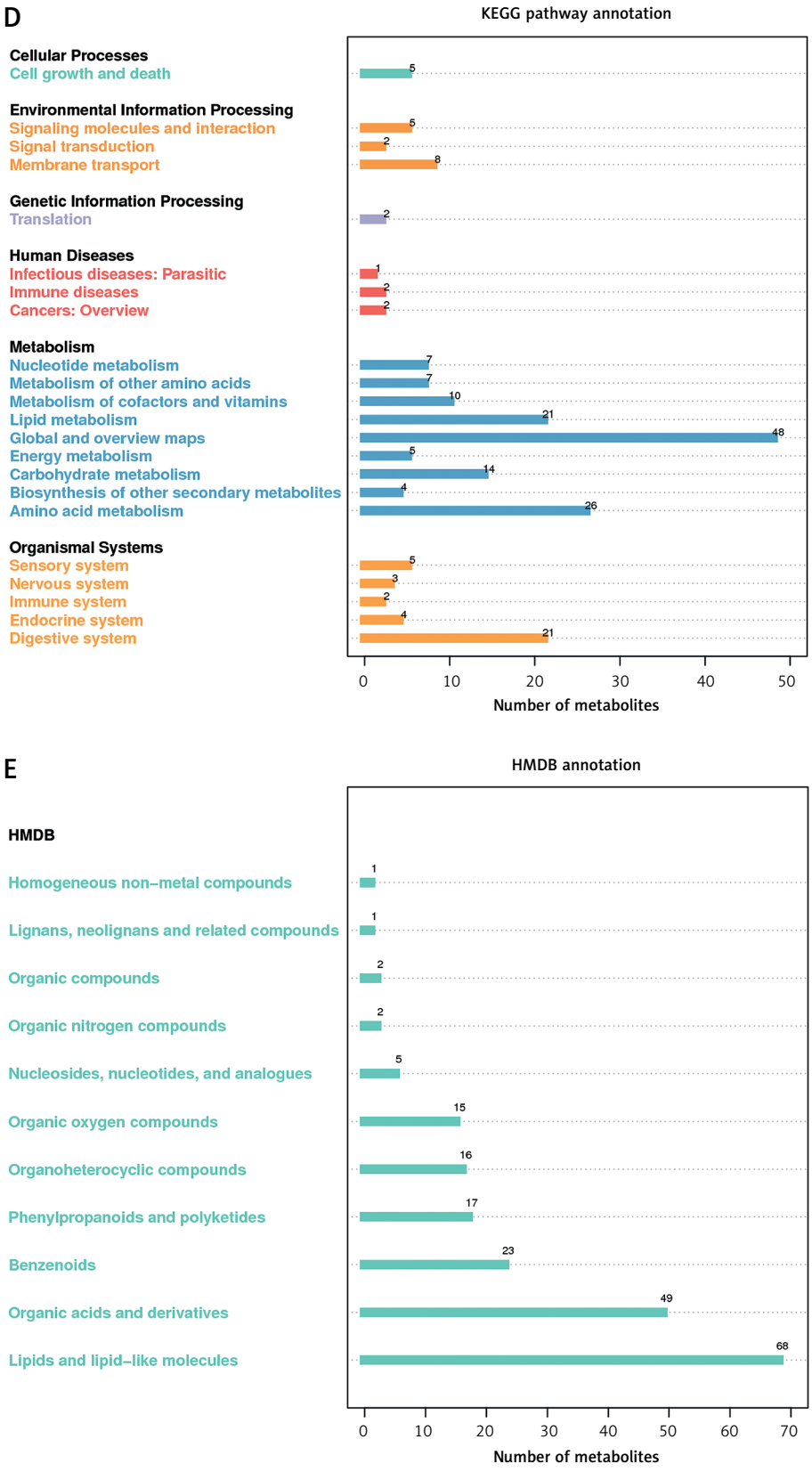


Figure 3. Cont. Metabolite annotation. **D** – KEGG pathway annotation (negative mode). **E** – HMDB annotation (negative mode)

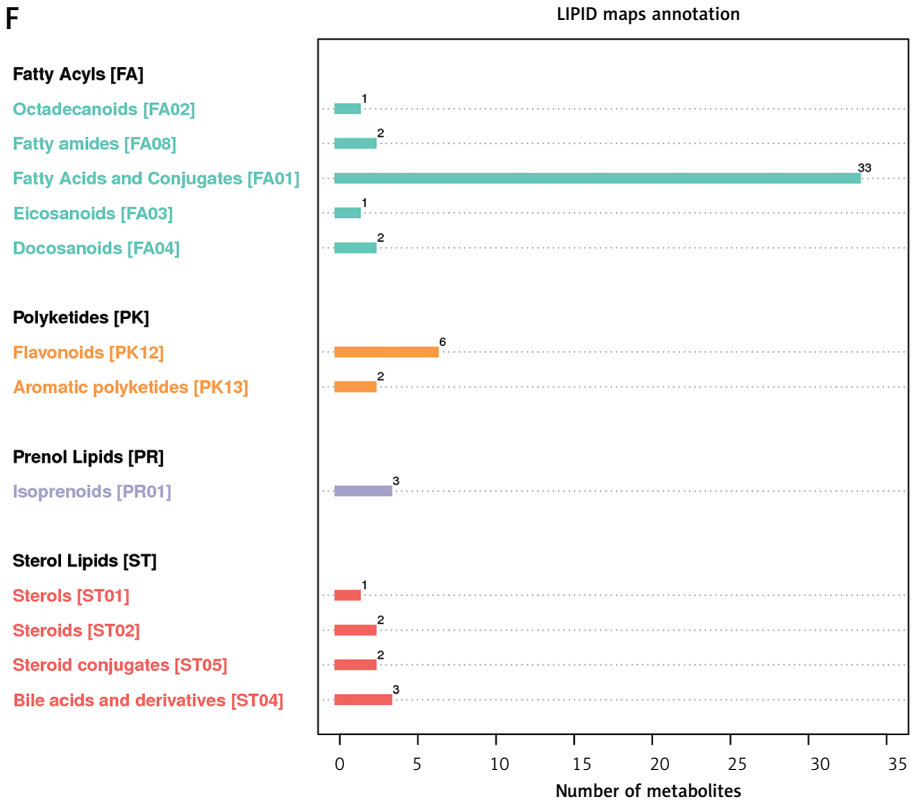


Figure 3. Cont. Metabolite annotation. **F** – LIPID maps annotation (negative mode)

were generally lower compared to the positive mode and were slightly above 0.65.

Discussion

Understanding the metabolic profiles of IgAN, MN, and DN is crucial for advancing dianostic precision, treatment effectiveness, and accurate prognosis in the field of nephrology. Detailed metabolic profiling facilitates accurate disease differentiation and identification of specific biomarkers, which may aid in the development of new early and precise diagnostic strategies [11]. Insights into the underlying pathophysiological mechanisms derived from these profiles can guide the development of targeted and personalized therapies, as well as monitoring of treatment responses. Furthermore, metabolic markers offer prognostic value by predicting disease progression and stratifying patient risk, which is essential for effective management [12, 13]. Researching metabolic pathways is important for advancing our understanding of nephropathies by revealing unique and shared pathways across different nephropathies, ultimately contributing to improved patient outcomes and scientific advancements [14].

Our study shows that there are distinct differences in metabolic profiles of IgAN, MN, and DN compared to healthy controls. Among 557 identified differential metabolites, only 118 (21.2%) were found in all three comparison groups. Differential metabolites of IgAN were significantly enriched in arachidonic acid metabolism, starch and sucrose metabolism, ferroptosis, and other pathways. Arachidonic acid metabolism plays a crucial role in kidney disorders and is associated with glomerular and interstitial inflammation [15]. Altered expression of metabolites responsible for arachidonic acid metabolism in IgAN was recently reported [16]. Interestingly, certain pathways, such as starch and sucrose metabolism, were mostly reported in studies investigating metabolic profiles of diabetes [17, 18]. However, in our case, starch and sucrose metabolism was impaired in the IgAN group rather than the DN group. In the DN group, differential metabolites were mainly enriched in phenylalanine, tyrosine and tryptophan biosynthesis, histidine metabolism, etc. Phenylalanine, tyrosine and tryptophan as well as histidine play important roles in glucose transport and metabolism. A recent study reported that higher expression levels of tyrosine but not phenylalanine or tryptophan were associated with an increased risk of DN in the Chinese population [19]. However, large cohort studies are needed to validate differences in expression levels of these aromatic amino acids between DN patients and healthy controls, as several studies obtained opposite results [20, 21]. Finally, MN-enriched pathways included steroid

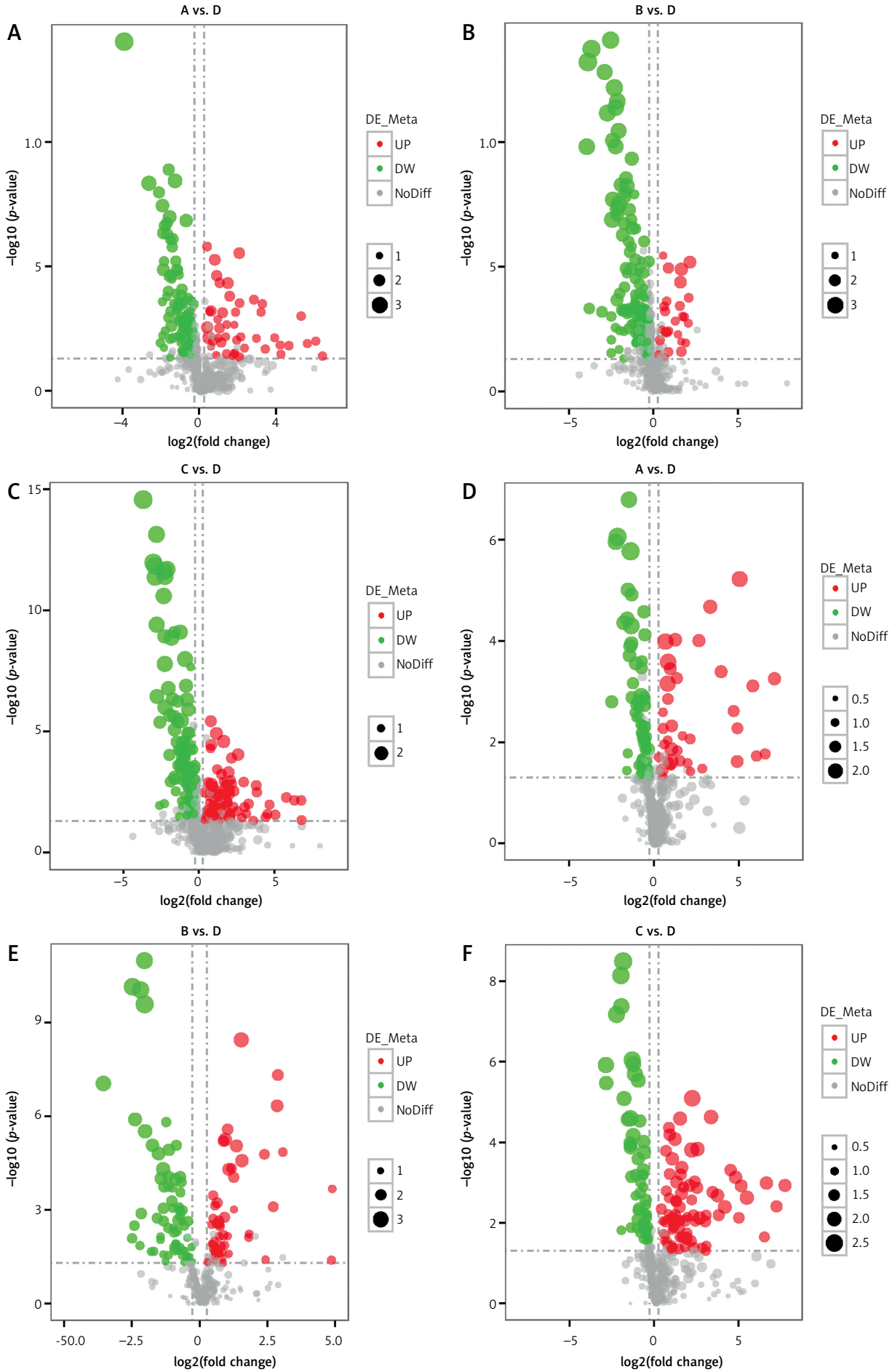


Figure 4. Volcano plots of metabolites. **A** – IgA nephropathy (IgAN) vs. control pair (positive mode). **B** – Membranous nephropathy (MN) vs. control pair (positive mode). **C** – Diabetic nephropathy (DN) vs. control pair (positive mode). **D** – IgAN vs. control pair (negative mode). **E** – MN vs. control pair (negative mode). **F** – DN vs. control pair (negative mode)

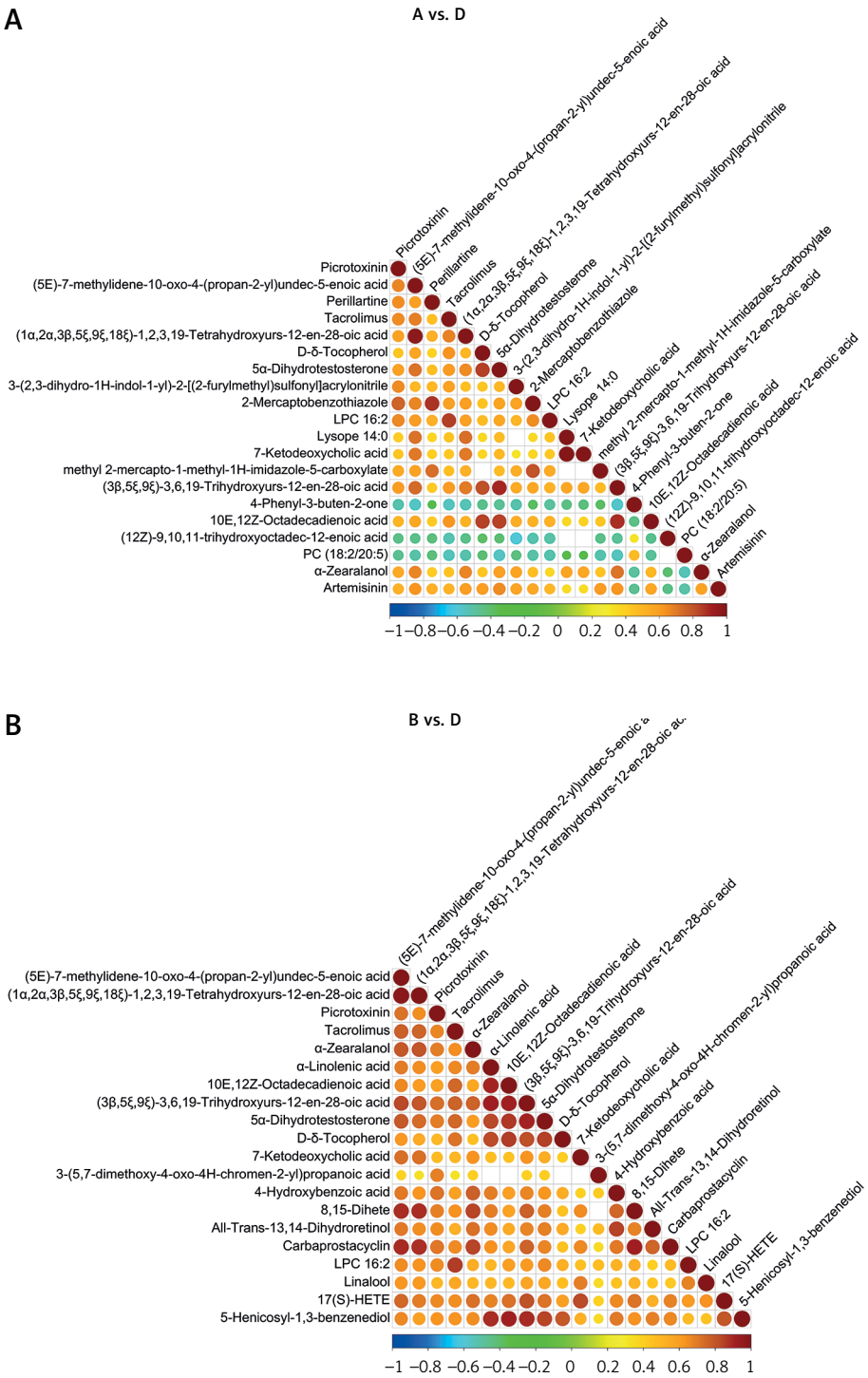


Figure 5. Correlation between differential metabolites. **A** – IgA nephropathy (IgAN) vs. control pair (positive mode). **B** – Membranous nephropathy (MN) vs. control pair (positive mode)

hormone biosynthesis, neuroactive ligand-receptor interaction, and bile secretion, which is consistent with several reports on metabolic profiles of IgAN and DN in animal and human models [22–25]. Specifically, altered bile secretion was discovered in rats with IgAN and DN mice with DN [22, 23]. Many kidney diseases are characterized by changes in bile acid levels in the plasma, kidney, and urine. Increased levels of bile acids are associated with oxidative damage of renal tubular cell membranes, which results in poor glomerular filtration rates and renal function [26].

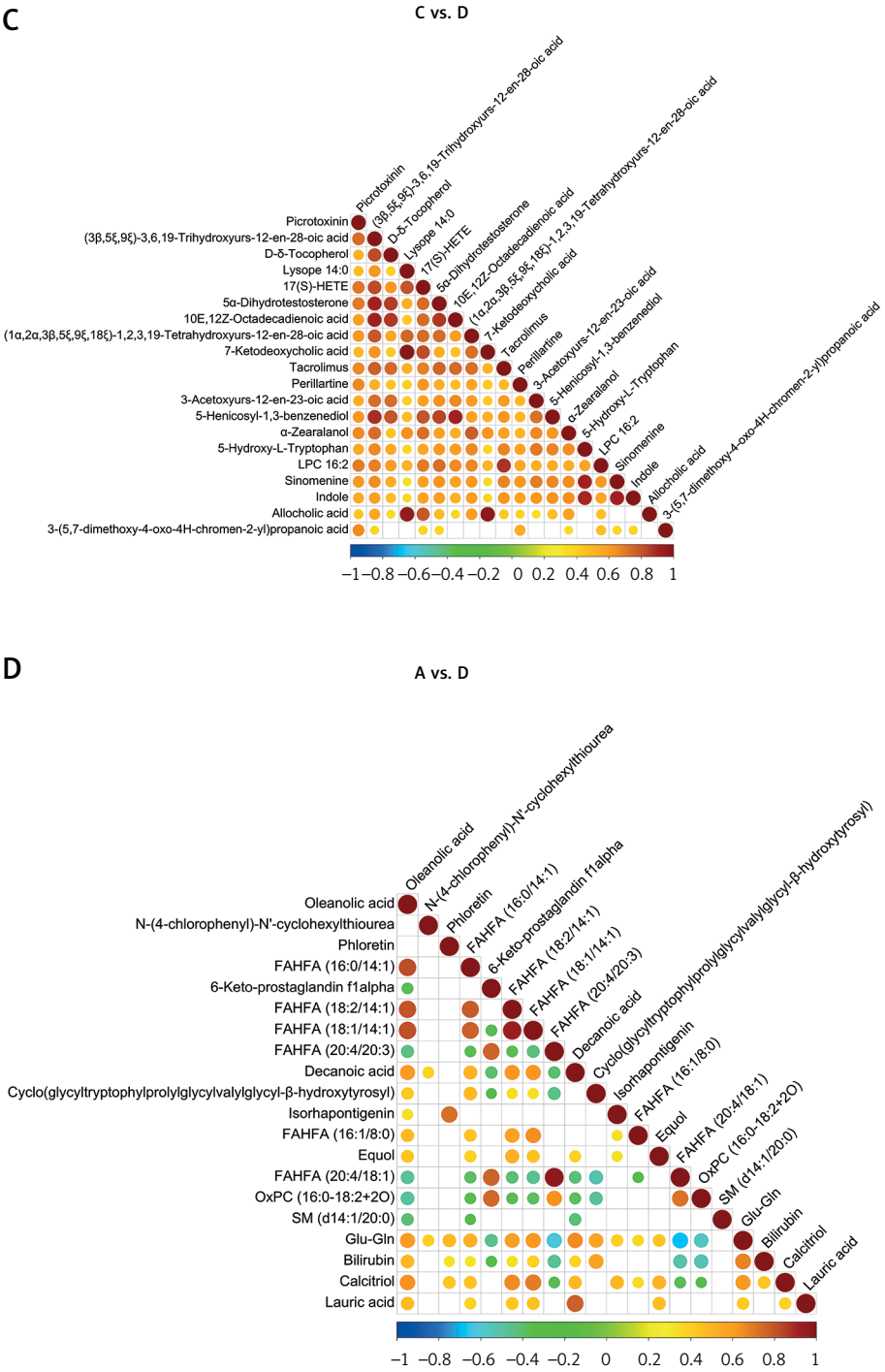


Figure 5. Cont. Correlation between differential metabolites. **C** – Diabetic nephropathy (DN) vs. control pair (positive mode). **D** – IgAN vs. control pair (negative mode)

The predictive modeling of differential metabolites using logistic regression has demonstrated varying levels of discriminatory ability across different nephropathy types when compared to controls. Our study analyzed the performance in both positive and negative ion modes, yielding various results for IgAN, MN, and DN. In the positive mode, the cumulative AUC values for IgAN vs. controls and MN vs. controls were 0.965 and 0.972, respectively. The strong performance characterized by near-perfect AUC values with high sensitivity and specificity in these comparison pairs highlights the potential of these metabolites as reliable biomarkers for IgAN and MN. In contrast, the AUC value for DN vs controls was 0.573, which is significantly lower and close to the performance

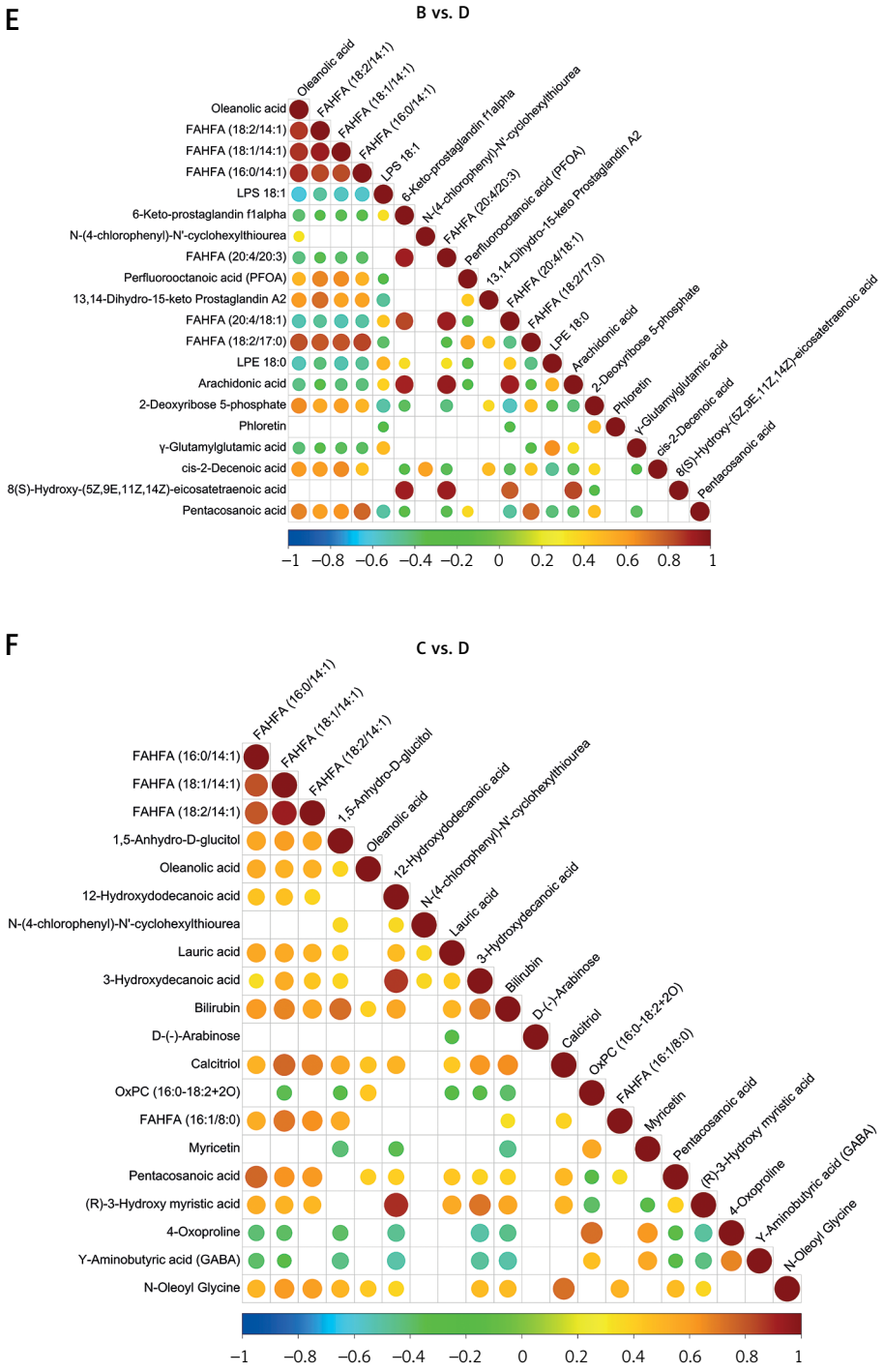


Figure 5. Cont. Correlation between differential metabolites. **E** – MN vs. control pair (negative mode). **F** – DN vs. control pair (negative mode)

of a random classifier (AUC = 0.5). This suggests that the metabolites identified in the positive mode are less effective in distinguishing DN from controls. The lower discriminatory ability may be due to the heterogeneous nature of DN or the overlapping metabolic features between DN and controls. Further investigation is needed to identify more specific biomarkers or to refine the metabolic profiling techniques for better differentiation of DN. The AUC values obtained in the negative ion mode were generally lower compared to the positive mode, with values slightly above 0.65 for all comparisons. Although these values indicate a moderate level of discriminatory power, they are not as high as those observed in the positive mode. The lower performance in

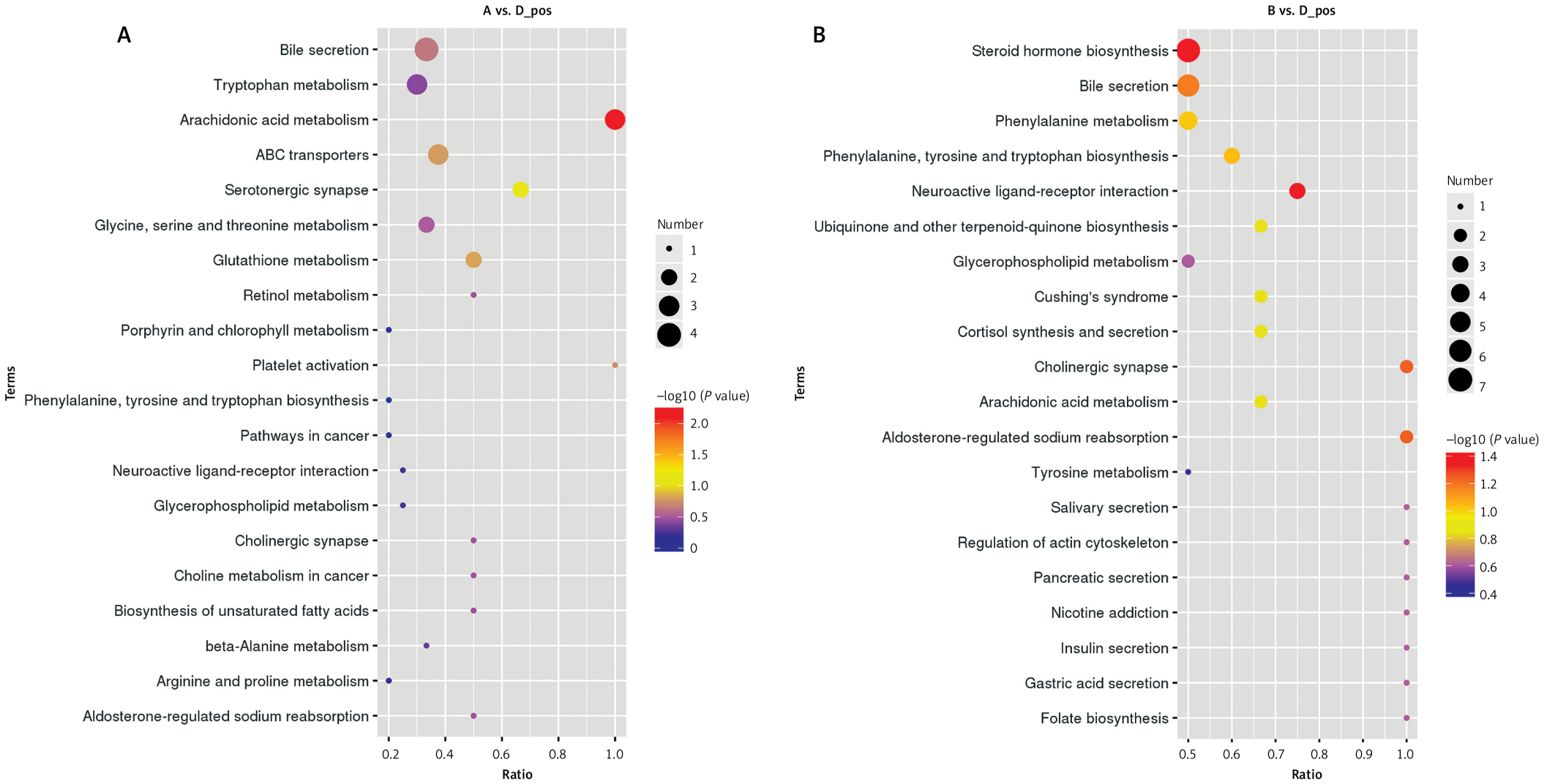


Figure 6. Kyoto Encyclopedia of Genes and Genomes (KEGG) enrichment analysis. **A** – IgA nephropathy (IgAN) vs. control pair (positive mode). **B** – Membranous nephropathy (MN) vs. control pair (positive mode)

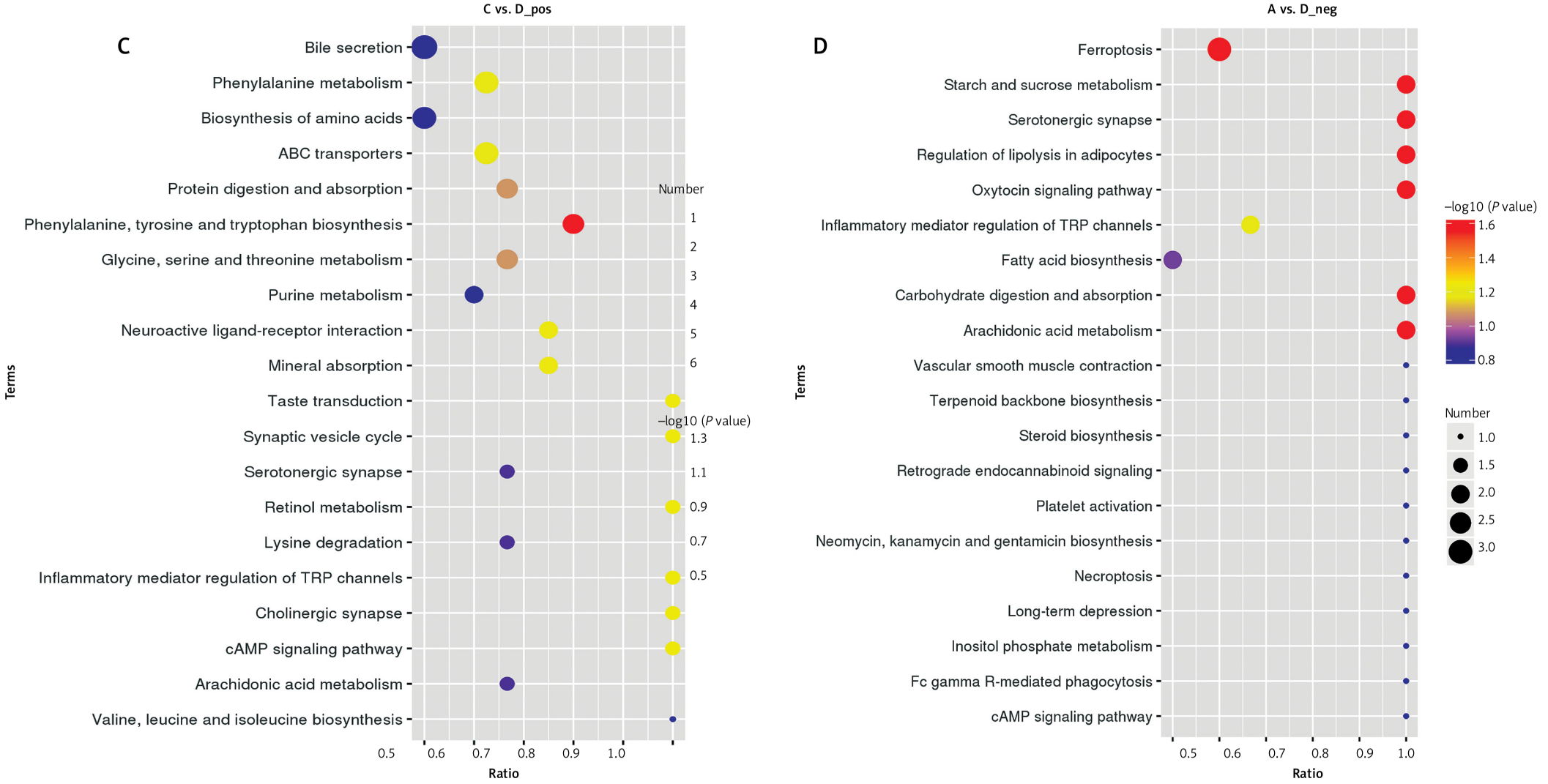


Figure 6. Cont. Kyoto Encyclopedia of Genes and Genomes (KEGG) enrichment analysis. **C** – Diabetic nephropathy (DN) vs. control pair (positive mode). **D** – IgAN vs. control pair (negative mode)

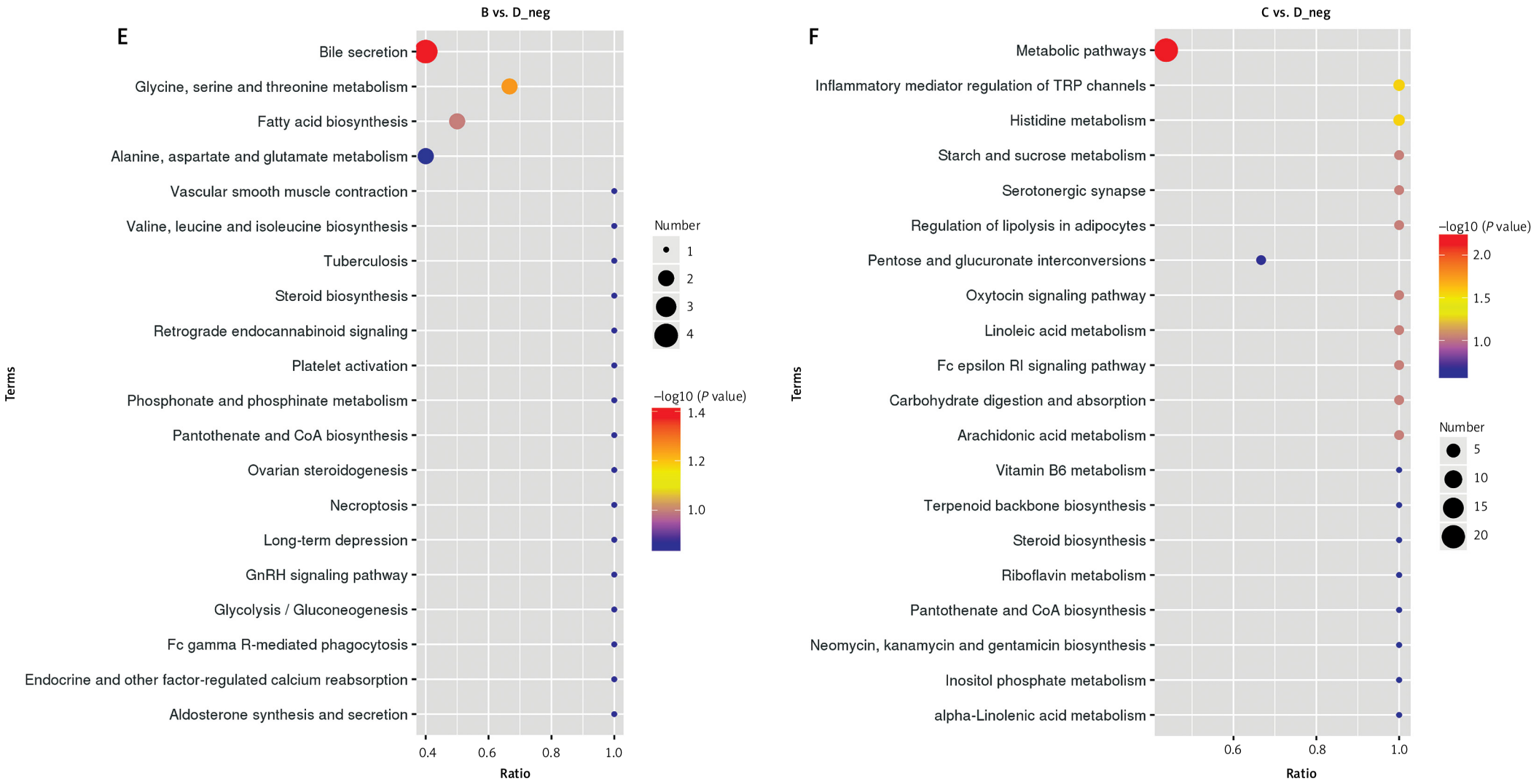


Figure 6. Cont. Kyoto Encyclopedia of Genes and Genomes (KEGG) enrichment analysis. **E** – MN vs. control pair (negative mode). **F** – DN vs. control pair (negative mode)

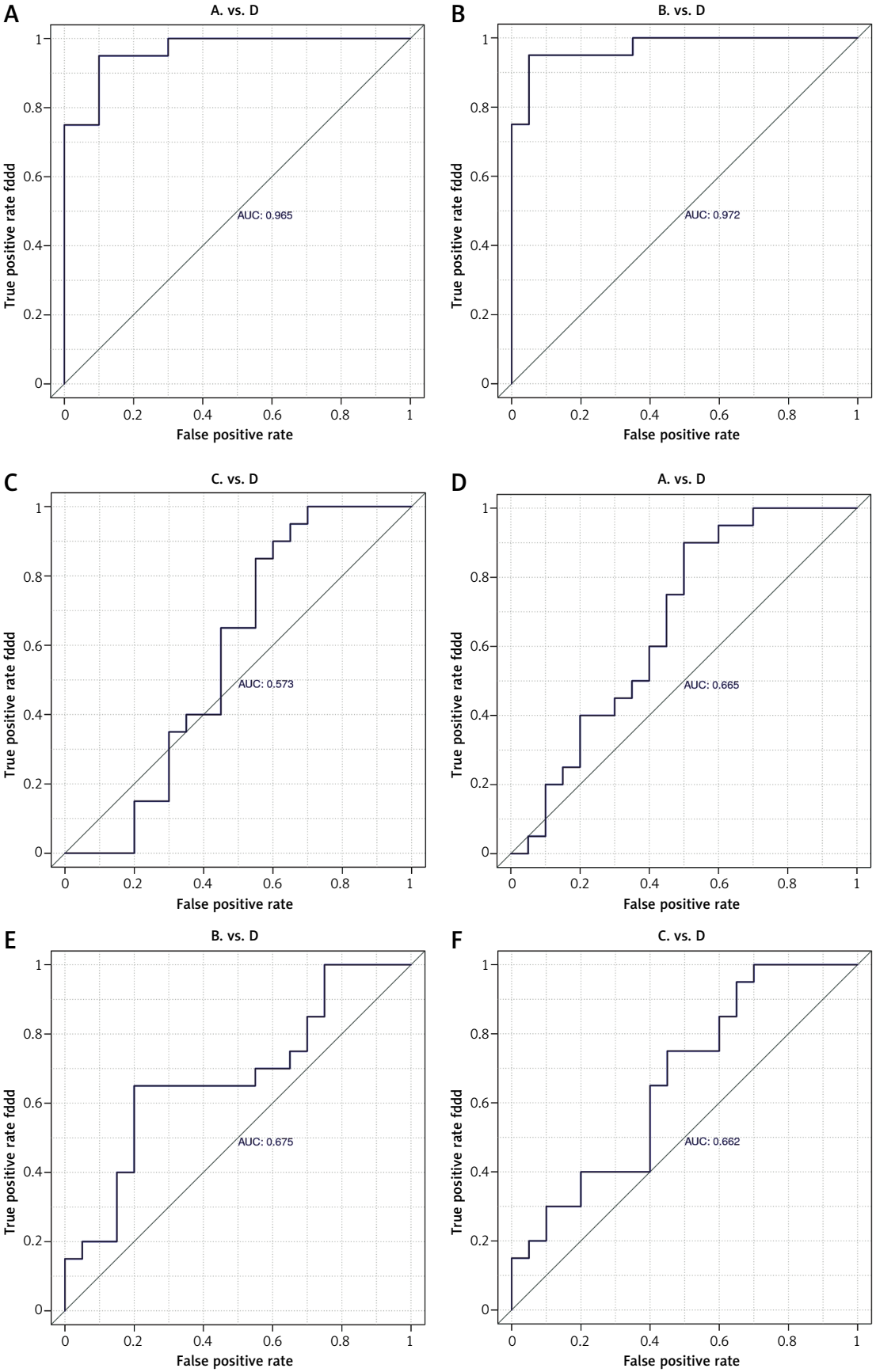


Figure 7. Receiver operating characteristic (ROC) curve of differential metabolites. **A** – IgA nephropathy (IgAN) vs. control pair (positive mode). **B** – Membranous nephropathy (MN) vs. control pair (positive mode). **C** – Diabetic nephropathy (DN) vs. control pair (positive mode). **D** – IgAN vs. control pair (negative mode). **E** – MN vs. control pair (negative mode). **F** – DN vs. control pair (negative mode)

the negative mode is likely attributed to differences between the modes, affecting the identification and quantification of metabolites [27–33]. All studies that analyzed differences in metabolic profiles of IgAN, MN, or DN that we were able to find calculated the predictive performance of one metabolite rather than reporting AUC of the combined model; therefore, we were unable to compare the results.

Our study has several limitations that warrant consideration. First, the small, single-center cohort (n = 20 per group) and strict exclusion criteria may limit the statistical power and applicability of our results to broader populations. Therefore, future multicenter studies with larger, demographically diverse cohorts are necessary to validate the findings and build robust, generalizable biomarker panels. Second, as this is a cross-sectional analysis, we could not assess the temporal stability or causality of identified biomarkers. Prospective longitudinal metabolomics studies are critical to understand biomarker kinetics, evaluate prognostic potential, and assess how metabolomic signatures evolve with therapeutic interventions. Third, the suboptimal performance of logistic regression models in positive mode, especially for DN, could be a result of incomplete metabolite coverage and sensitivity of the LC-MS system. Future studies should employ dual-mode ionization, untargeted and targeted LC-MS/MS, and integrative platforms (e.g., NMR + MS) to enhance metabolome coverage and improve detection sensitivity across nephropathy types. Fourth, our study did not account for potential confounders, such as unrecorded comorbidities and genetic background. These confounders can influence metabolic profiles and may differ between nephropathy subtypes. Metabolomic analyses should be integrated with comprehensive clinical metadata, including genetic, pharmacological, and lifestyle information. Statistical techniques such as multivariable regression, mixed-effects modeling, and propensity score matching can further help mitigate confounding effects. Future studies can use multi-omic integration (e.g., transcriptomics, proteomics) and tissue specific pathway analysis (e.g., using Reactome or kidney-specific metabolic atlases) to improve biological interpretability and enhance mechanistic understanding. In conclusion, the excellent performance of the predictive models in the positive mode for IgAN and MN underscores the potential clinical application of the metabolic biomarkers for early diagnosis and monitoring. However, the suboptimal performance for DN, particularly in the positive mode, clearly shows the need for further research to improve the metabolic profiling and identification of specific biomarkers for DN. Future studies should focus on optimizing the metabolomic analysis protocols, potentially integrating both ionization modes, to enhance the overall predictive accuracy. Moreover, expanding the sample size and including a broader range of metabolites could improve the accuracy and generalizability of the predictive models.

In conclusion, IgAN, MN, and DN have similar but distinct metabolic profiles. Only positive node metabolites of IgAN and MN exhibited high predictive performance.

Supplementary materials

The following supporting information can be downloaded at: https://zenodo.org/doi/10.5281/zenodo.13224489 Supplementary Figure S1. Quality control analysis: A – Pearson correlation between quality control samples (positive mode); B – principal component (PC) plot of five groups (positive mode, 2 dimensions); C – PC plot of five groups (positive mode, 3 dimensions); D – Pearson correlation between QC samples (negative mode); E – PC plot of five groups (negative mode, 2 dimensions); F – PC plot of five groups (negative mode, 3 dimensions). Supplementary Figure S2. Heatmaps of differential metabolites: A – IgA nephropathy (IgAN) vs control pair (positive mode); B – membranous nephropathy (MN) vs. control pair (positive mode); (C) diabetic nephropathy (DN) vs. control pair (positive mode); (D) IgAN vs. control pair (negative mode); (E) MN vs. control pair (negative mode); (F) DN vs. control pair (negative mode). Supplementary Table SI. List of differential metabolites in three comparison pairs (positive mode). Supplementary Table SII. List of differential metabolites in three comparison pairs (negative mode). Supplementary Table SIII. KEGG enrichment pathways.

Funding

This work was supported by the Key Laboratory Project of Shanxi Province, grant number 201805D111020, and the Key Laboratory Construction Plan Project of Shanxi Provincial Health Commission, grant number 2020SYS01.

Ethical approval

The study was conducted in accordance with the Declaration of Helsinki and approved by the Ethics Committee of Shanxi Provincial People's Hospital, Shanxi Medical University.

Conflict of interest

The authors declare no conflict of interest.

References

1. Vahedian-Azimi A, Beni FH, Fras Z, et al. Effects of statins on the incidence and outcomes of acute kidney

injury in critically ill patients: a systematic review and meta-analysis. Arch Med Sci 2023; 19: 952-64.
2. Katsiki N, Kolovou G, Melidonis A, Banach M. The Cardiac-Kidney-Liver (CKL) syndrome: the "real entity" of type 2 diabetes mellitus. Arch Med Sci 2024; 20: 207-15.
3. Guo X, Tie X, Zhang Y, et al. Management and clinical outcomes of membranous nephropathy, IgA nephropathy, and minimal change disease two years post-kidney biopsy. Kidney Blood Press Res 2024; 49: 345-54.
4. Stamellou E, Seikrit C, Tang SCW, et al. IgA nephropathy. Nat Rev Dis Primers 2023; 9: 67.
5. Nieto-Gañán I, Iturrieta-Zuazo I, Rita C, Carrasco-Sayalero Á. Revisiting immunological and clinical aspects of membranous nephropathy. Clin Immunol 2022; 237: 108976.
6. Fox CS, Matsushita K, Woodward M, et al. Associations of kidney disease measures with mortality and end-stage renal disease in individuals with and without diabetes: a meta-analysis. Lancet 2012; 380: 1662-73.
7. Furlani IL, da Cruz Nunes E, Canuto GAB, Macedo AN, Oliveira RV. Liquid chromatography-mass spectrometry for clinical metabolomics: an overview. Adv Exp Med Biol 2021; 1336: 179-213.
8. Pereira PR, Carrageta DF, Oliveira PF, Rodrigues A, Alves MG, Monteiro MP. Metabolomics as a tool for the early diagnosis and prognosis of diabetic kidney disease. Med Res Rev 2022; 42: 1518-44.
9. Wang H, Ainiwaer A, Song Y, et al. Perturbed gut microbiome and fecal and serum metabolomes are associated with chronic kidney disease severity. Microbiome 2023; 11: 3.
10. Harvey FC, Collao V, Bhattacharya SK. High-resolution liquid chromatography-mass spectrometry for lipidomics. Methods Mol Biol 2023; 2625: 57-63.
11. González-DomínguezÁ, Armeni M, Savolainen O, Lechuga-Sancho AM, Landberg R, González-Domínguez R. Untargeted metabolomics based on liquid chromatography-mass spectrometry for the analysis of plasma and erythrocyte samples in childhood obesity. Methods Mol Biol 2023; 2571: 115-22.
12. Saucedo AL, Perales-Quintana MM, Paniagua-Vega D, Sanchez-Martinez C, Cordero-Perez P, Minsky NW. Chronic kidney disease and the search for new biomarkers for early diagnosis. Curr Med Chem 2018; 25: 3719-47.
13. Li H, Li D, Ledru N, et al. Transcriptomic, epigenomic, and spatial metabolomic cell profiling redefines regional human kidney anatomy. Cell Metab 2024; 36: 1105-25.e10.
14. Lecamwasam A, Mansell T, Ekinci EI, Saffery R, Dwyer KM. Blood plasma metabolites in diabetes-associated chronic kidney disease: a focus on lipid profiles and cardiovascular risk. Front Nutr 2022; 9: 821209.
15. Fromentin S, Forslund SK, Chechi K, et al. Microbiome and metabolome features of the cardiometabolic disease spectrum. Nat Med 2022; 28: 303-14.
16. Uwaezuoke SN, Muoneke UV, Mbanefo NR. The supportive treatment of IgA nephropathy and idiopathic nephrotic syndrome: how useful are omega-3 polyunsaturated fatty acids? Int J Nephrol Renovasc Dis 2020; 13: 27-35.
17. Wu H, Tang D, Yun M, et al. Metabolic dysfunctions of intestinal fatty acids and tryptophan reveal immuno-inflammatory response activation in IgA nephropathy. Front Med 2022; 9: 811526.
18. Cui C, Wang C, Han S, Yu D, Zhu L, Jiang P. Impact of a long-term high-fructose diet on systemic metabolic profiles of mice. FASEB Bioadv 2022; 4: 560-72.
19. Wang X, He Q, Chen Q, et al. Network pharmacology combined with metabolomics to study the mechanism of Shenyan Kangfu Tablets in the treatment of diabetic nephropathy. J Ethnopharmacol 2021; 270: 113817.
20. Zhang S, Li X, Luo H, Fang ZZ, Ai H. Role of aromatic amino acids in pathogeneses of diabetic nephropathy in Chinese patients with type 2 diabetes. J Diabetes Complications 2020; 34: 107667.
21. Luo HH, Li J, Feng XF, et al. Plasma phenylalanine and tyrosine and their interactions with diabetic nephropathy for risk of diabetic retinopathy in type 2 diabetes. BMJ Open Diabetes Res Care 2020; 8: e000877.
22. Liu Y, Chen X, Liu Y, et al. Metabolomic study of the protective effect of Gandi capsule for diabetic nephropathy. Chem Biol Interact 2019; 314: 108815.
23. Zhao J, He K, Du H, et al. Bioinformatics prediction and experimental verification of key biomarkers for diabetic kidney disease based on transcriptome sequencing in mice. PeerJ 2022; 10: e13932.
24. Li J, Cao Y, Lu R, et al. Integrated fecal microbiome and serum metabolomics analysis reveals abnormal changes in rats with immunoglobulin a nephropathy and the intervention effect of Zhen Wu Tang. Front Pharmacol 2020; 11: 606689.
25. Xue R, Wang Y, Geng L, et al. Comprehensive analysis of the gene expression profile of the male and female BTBR mice with diabetic nephropathy. Int J Biol Macromol 2024; 257: 128720.
26. Ren H, Lv W, Shang Z, et al. Identifying functional subtypes of IgA nephropathy based on three machine learning algorithms and WGCNA. BMC Med Genomics 2024; 17: 61.
27. Yang J, Pontoglio M, Terzi F. Bile acids and Farnesoid X Receptor in renal pathophysiology. Nephron 2024; 148: 618-30.
28. Niessen WM. Fragmentation of toxicologically relevant drugs in positive-ion liquid chromatography-tandem mass spectrometry. Mass Spectrom Rev 2011; 30: 626-63.
29. Niessen WM. Fragmentation of toxicologically relevant drugs in negative-ion liquid chromatography-tandem mass spectrometry. Mass Spectrom Rev 2012; 31: 626-65.
30. Ye M, Tang D, Li W, et al. Serum metabolomics analysis reveals metabolite profile and key biomarkers of idiopathic membranous nephropathy. PeerJ 2023; 11: e15167.
31. Dong L, Tan J, Zhong Z, Tang Y, Qin W. Altered serum metabolic profile in patients with IgA nephropathy. Clin Chim Acta 2023; 549: 117561.
32. Lin HT, Cheng ML, Lo CJ, Lin G, Liu FC. Metabolomic signature of diabetic kidney disease in cerebrospinal fluid and plasma of patients with type 2 diabetes using liquid chromatography-mass spectrometry. Diagnostics 2022; 12: 2626.
33. Liu S, Gui Y, Wang MS, et al. Serum integrative omics reveals the landscape of human diabetic kidney disease. Mol Metab 2021; 54: 101367.